Baksheev, I.A., Beliatsky, B.V. Sm-Nd and Rb-Sr isotopic systems of sheelite from Beresovskoe Au-bearing deposit (Middle Urals) // Lithosphere, 2011. No. 4. P. 110–118 [in Russian].

Bea, F. et al. Recycling of continental crust into the mantle as revealed by Kytlymdunite zircons, Ural Mts, Russia. Terra Nova, 2001. Vol. 13. P. 407–412.

Beane, R.J., Connelly, J.N. $^{40}Ar/^{39}Ar$, U-Pb, and Sm-Nd constraints on the timing of metamorphic events in the Maksyutov Complex, southern Ural Mountains // Journal of Geol. Society, 2000. Vol. 157. P. 811–822.

Bjorlykke, A., Vokes, F.M., Birkeland, A., Thorpe, R.I. Lead isotope systematics of strata-bound sulfide deposits in the Caledonides of Norway // Economic Geology, 1993. Vol. 88. P. 397–417.

Brown, D., Herrington, R.J., Alvarez-Marron, J. Processes of Arc-Continent Collision in the Uralides // In: Brown D and Ryan PD (eds) Arc-Continent collision. Springer-Verlag, Berlin Heidelberg, 2011. P. 311–340.

Buslaev, F.P., Kaleganov, B.A. The age of sulfide-ore formation according to the K/Ar method // In: Prokin VA and Buslaev FP (eds) Copper-sulfide deposits of the Urals: Conditions of formation. Russian Academy of Science, Ural Branch, Ekaterinburg, 1992. P. 186-199 [in Russian].

Fershtater, G.B., Krasnobaev, A.A., Bea, F., Montero, P., Borodina, N.S. Geodynamic settings and history of the Paleozoic intrusive magmatism of the Central and Southern Urals: Results of Zircon Dating // Geotectonics, 2007. Vol. 41. P. 465–486.

Gannoun, A. et al. Re–Os isotopic constraints on the genesis and evolution of the Dergamish and Ivanovka Cu (Co, Au) massive sulphide deposits, south Urals, Russia // Chem. Geol., 2003. Vol. 196. P. 193–207.

Herrington, R.J., Brown, D. The generation and preservation of mineral deposits in arc-continent collision environment // In: Brown D and Ryan PD (eds) Arc-Continent collision, Springer-Verlag, Berlin Heidelberg, 2011. P. 145–162.

Hu, R.-Z., Wei, W.-F., Bi, X.-W., Peng, J.-T., Qi, Y.-Q., Wu, L.-Y., Chen, Y.-W. Molybdenite Re-Os and muscovite 40Ar/ 39Ar dating of the Xihuashan tungsten deposit, central Nanling district, South China // Lithos, 2012. Vol. 150. P. 111–118.

Huston, D.L., Pehrsson, S., Eglington, B.M., Zaw, K. The Geology and Metallogeny of Volcanic-Hosted Massive Sulfide Deposits: Variations through Geologic Time and with Tectonic Setting // Econ. Geol., 2010. Vol. 105. P. 571–591.

Maslennikov, V.V., Maslennikova, S.P., Large, R.R., Danyushevsky, L.V. Study of Trace Element Zonation in Vent Chimneys from the Silurian Yaman-Kasy Volcanic-Hosted Massive Sulfide Deposit (Southern Urals, Russia) Using Laser Ablation-Inductively Coupled Plasma Mass Spectrometry (LA-ICPMS) // Econ. Geol., 2009. Vol. 104. P. 1111–1141.

Smirnov, V.N., Fadeicheva, I.F., Ivanov, K.S. Geochemistry of Volcanic Rocks in the Tagil Zone of the Urals as an Indicator of Geodynamic Environments of Their Formation // Doklady Earth Sciences, 2008. Vol. 423 (8). P. 1278–1281.

Tessalina, S.G. et al. Osmium isotope distribution within the Palaeozoic Alexandrinka seafloor hydrothermal system in the Southern Urals, Russia // Ore Geol. Rev., 2008. Vol. 33. P. 70–80.

Yazeva, R.G., Bochkarev, V.V. Silurian island arc of the Urals: structure, evolution and geodynamics // Geophysics, 1996. Vol. 29 (6). P. 478–489.

F.J. Testa, D.R. Cooke
CODES, University of Tasmania, Hobart, Australia, F.J.Testa@utas.edu.au

PRELIMINARY THERMODYNAMIC MODEL FOR Bi-MINERALS IN THE SAN FRANCISCO DE LOS ANDES Bi-Cu-Au BRECCIA PIPE, SAN JUAN, ARGENTINA

Комплексное месторождение Bi-Cu-Pb-Zn-Mo-As-Fe-Ag-Au Сан Франциско де Лос Андес располагается на восточном фланге Передового Хребта и представляет собой тело брекчий с турмалиновым цементом, возраст которого определяется пермским или более молодым магматизмом. Продуктивная минерализация представлена сульфидами, сульфосолями, теллуридами и самородными элементами и различается для разных участков месторождения, в основном содержаниями галенита и халькопирита и соответствующим уровнем примесей меди и свинца в висмутовых минералах, среди которых установлены висмутин, тетрадимит, промежуточные члены рядов висмутин-айкинит, крупкаит-паарит, зальцбурит-гледит. На основе термодинами-

ческого анализа делается вывод о том, что различия в минерализации на участках месторождения зависят в большей степени от активности растворенных Pb и Cu, чем от фугитивностей серы и теллура.

Introduction

San Francisco de los Andes mine (30?50?08??S – 69?35?58??W) is located on the eastern flank of the Cordillera Frontal, San Juan province, Argentina. The Cordillera Frontal is a geological province on the eastern flank of Cordillera de los Andes that extends from northern San Juan to southern Mendoza. The orebody is hosted by a tourmaline-cemented breccia pipe that has cut carboniferous sedimentary rocks [Llambias et al., 1969]. The sedimentary rocks have been intruded by the Tocota Pluton, a Permian intrusive complex that ranges from tonalite to granite in composition. Geochronological studies are currently being conducted in order to determine whether the breccia pipe is related to Permian or younger magmatism.

San Francisco de los Andes is characterized by complex Bi-Cu-Pb-Zn-Mo-As-Fe-Ag-Au mineralization, including native elements, sulfides, and sulfosalts. This article reports the occurrence of two different Bi-Cu-Pb mineral assemblages at opposite sides of the NW-SE trending elliptical breccias pipe. By means of detailed analytical studies and the available fluid inclusion data a preliminary thermodynamic model was developed for both assembles at a minimum temperature of 230 °C and a maximum temperature of 400 °C. It was aimed to constrain tentative fS_2 and fTe_2 values for the hydrothermal solutions using the previously determined sulfide and telluride assemblages.

Bi-Pb-(Cu) and Bi-Cu-(Pb) assemblages

Backscattered electron images (BSEI) were used to detect different mineral species, electron microprobe analyses (EMPA) to determine the major chemical compositions of each phase and laser ablation inductively coupled plasma mass spectrometry (LA-ICP-MS) to characterize their trace element geochemistry and mineral inclusion compositions.

Two apparently homogeneous bismuthinite crystals were chosen from each area. In both cases, a spot profile was drawn perpendicular to the main cleavage direction (010). Consecutive analyses were performed at 500 ?m intervals along the profile. The polished blocks were prepared from a sample of bismuthinite-cosalite cemented breccia (NW area) and bismuthinite-chalcopyrite cemented breccia (SE area).

Two distinct mineral species were identified from the 26 spots analyzed In the NW polished sample (Table). Fifteen out of the twenty six analyses correspond to bismuthinite ($Bi_{1.981}$ $Sb_{0.040}$) ($Pb_{0.025}$) ($Cu_{0.028}$ $Ag_{0.001}$) ($S_{2.986}$ $Se_{0.012}$ $Te_{0.002}$) No apparent chemical variations within the bismuthinite-aikinite solid solution series were detected. Bi contents are two orders of magnitude higher than Pb and Sb, three times higher than Cu and four orders of magnitude higher than Se and Te. Silver telluride inclusions are regularly spread within bismuthinite crystal. Argentocuprocosalite ($Pb_{1.663}$ $Cu_{0.326}$ $Ag_{0.240}$) ($Bi_{2.057}$ $Sb_{0.092}$) ($S_{4.976}$ $Se_{0.013}$ $Te_{0.011}$) was detected from nine EMPA analyses along the twenty-six-spot-profile. The term argentocuprocosalite is applied here to Ag- + Cu-bearing cosalite in order to explain the shift away from pure end-member cosalite as plotted on Fig. 1. The Bi and Pb signals from an LA-ICPMS analysis of argentocuprocosalite are two orders of magnitude higher than Ag, Sb and Cu and four to five times higher than Cd, Te, In, Se, Tl and Mn. No silver telluride inclusion was detected in this mineral. The two remaining analysis out of the 26 spots revealed two unclassified species.

Two recurrent mineral phases were found from the 35 spots analyzed In the SE polished sample (Table). Twenty four analyses determined that the species correspond to bismuthinite (Bi2.023 $Sb_{0.024}$) ($Pb_{0.022}$) ($Cu_{0.026}$ $Ag_{0.001}$) ($S_{2.972}$ $Se_{0.015}$ $Te_{0.012}$) No apparent chemical variations within the bismuthinite-aikinite solid solution series were detected. Seven out of thirty five EMPA analyses match with tetradymite inclusions ($Bi_{2.037}$ $Sb_{0.016}$) ($Pb_{0.001}$) ($Cu_{0.009}$ $Ag_{0.011}$) ($Te_{1.876}$ $S_{1.096}$ $Se_{0.028}$). The remaining four spots belong to four different members within the bismuthinite-aikinite solid solution series: Friedrichite ($Pb_{4.802}$) ($Cu_{4.939}$ $Ag_{0.032}$) ($Bi_{7.166}$ $Sb_{0.305}$) ($S1_{7.961}$ $Se_{0.026}$ $Te_{0.013}$), two species between the krupkaite-paarite members with the following chemical composition ($Pb_{0.911}$) ($Cu_{1.135}$ $Ag_{0.013}$) ($Bi_{3.094}$ $Sb_{0.012}$) ($S_{5.969}Se_{0.025}$ $Te_{0.006}$) and ($Pb_{0.891}$) ($Cu_{0.894}$ Ag_0) ($Bi_{3.121}$ $Sb_{0.045}$) ($S_{5.975}$ $Se_{0.019}$ Te0.006) and a mineral phase within salzburgite-gladite members ($Pb_{1.482}$) ($Cu_{1.475}$ Ag_0) ($Bi_{6.624}$ $Sb_{0.096}$) ($S_{11.945}$ $Se_{0.047}$ $Te_{0.008}$).

Table

EMPA mean chemical composition of each species

	NW Area				SE Area					
							Bismuthinite-aikinite solid solution series n=4			
	Bismuthinite n=15	Ag-Cu cosalite n=09	Unknown n=01	Unknown n=01	Bismuthinite n=24	Tetradymite n=07	Gladite-salzburgite member n=01	Paarite-krupkaite member n=01	n=01	Friedrichite n=01
Bi	79.31	43.33	47.56	40.49	79.46	60.81	63.04	59.63	58.52	43.62
Sb	0.93	1.13	0.55	1.68	0.55	0.27	0.53	0.50	0.14	1.08
Pb	0.99	34.74	20.95	26.09	0.84	0.03	13.98	16.88	17.09	28.98
Cu	0.34	2.09	6.71	7.53	0.31	0.08	4.27	5.20	6.53	9.14
Ag	0.01	2.61	7.58	6.56	0.02	0.17	0.00	0.00	0.13	0.10
S	18.34	16.08	16.74	16.62	17.91	5.02	17.44	17.52	17.32	16.78
Se	0.18	0.11	0.19	0.18	0.23	0.31	0.17	0.14	0.18	0.06
Te	0.06	0.14	0.18	0.21	0.30	34.18	0.04	0.07	0.07	0.05
∑	100.16	100.23	100.46	99.37	99.62	100.89	99.48	99.93	99.98	99.81

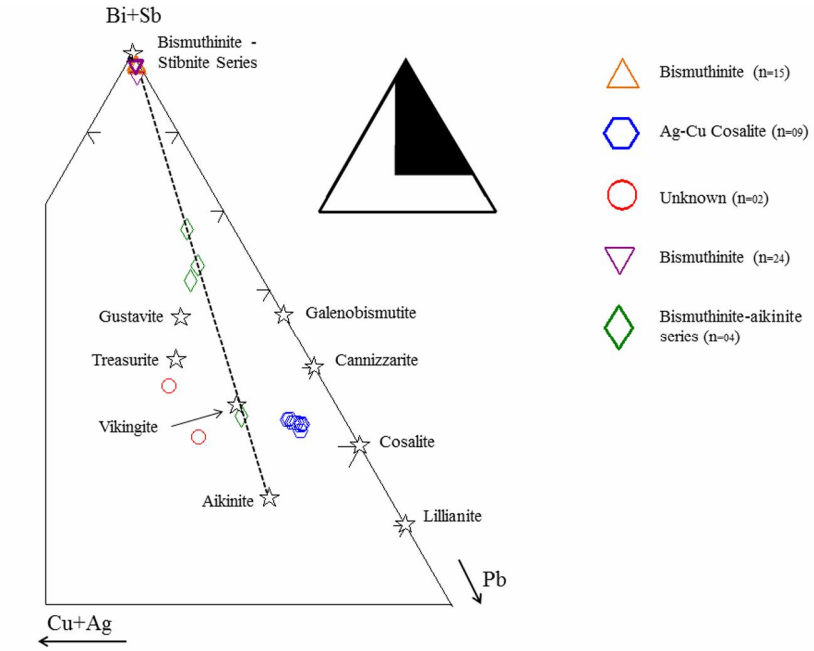

Fig. 1. (Cu+Ag)-(Bi+Sb)-Pb ternary diagram. Only sulfides and sulfosalts analyses are plotted.

Fluid inclusions

Little has been published on the conditions of formation of the San Francisco de los Andes deposit. The only data available are provided in a report by Cardo et. al [2008]. They estimated temperatures between 227 °C to 229 °C and a salinity of 14.6 wt % NaCl equiv for the two-phase, liquid-rich fluid inclusions found in quartz samples. Temperatures as high as 367 °C to 388 °C and salinities up to 45 wt % NaCl equiv were reported for the three–phase (liquid+vapor +halite) quartz-hosted fluid inclusions.

These temperatures are comparable with well documented tourmaline-breccia hosted Cu-Mo deposits such as Rio Blanco-Los Bronces [Frikken et al., 2005]. Measured homogenization temperature for Type ia (two-phase, liquid-rich fluid inclusions) and type iia (three-phases, salt saturated, halite-bearing fluid inclusions) range between less than 200 °C and more than 400 °C.

A thorough fluid inclusion study in the quartz and tourmaline hydrothermal cement from San Francisco de los Andes breccias will be conducted in the near future.

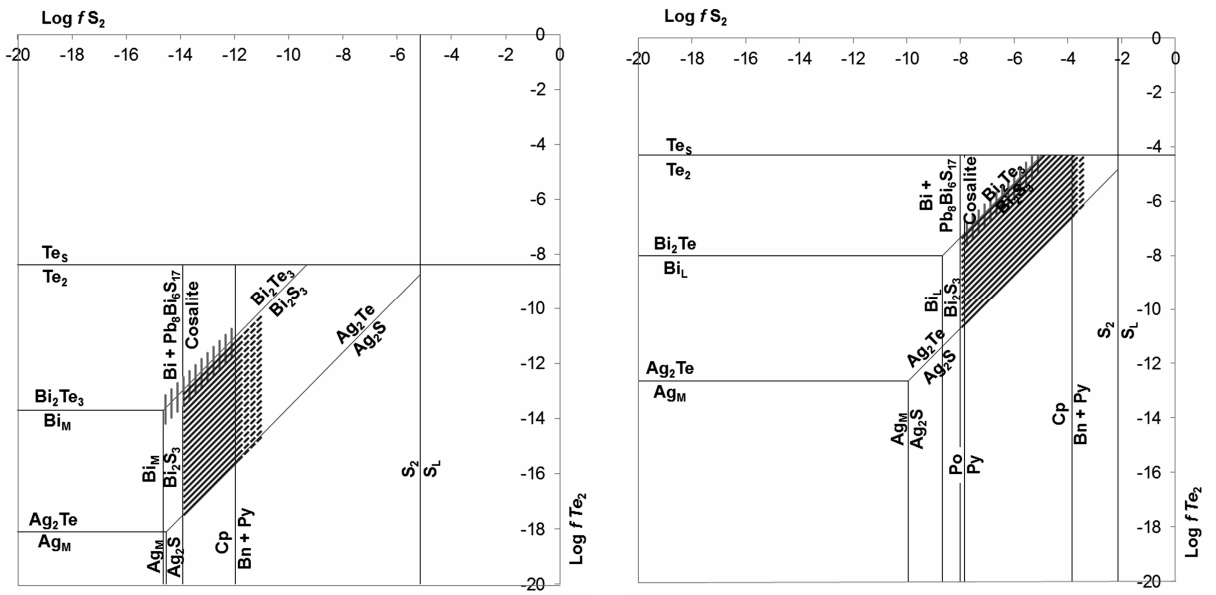

Fig. 2. fS_2-fTe_2 diagrams calculated at 230 °C (left) and 400 °C (right).

Preliminary thermodynamic model

Both mineral assemblages stability limits were calculated using thermochemical data from Afifi, Kelly and Essene [1988], Barton and Skinner [1967, 1979], Craig and Barton [1973], Garrels and Christ [1965], Krauskopf and Bird [1995] and Robie and Waldbaum [1968]. Each linear equation was calculated at two extreme temperatures (230 °C and 400 °C) and was plotted in fS_2-fTe_2 diagrams as it can be seen in Figure 2.

The stability field for the bismuthinite (Bi_2S_3) – hessite (Ag_2Te) – cosalite ($Pb_2Bi_2S_5$) assemblage is shown as diagonal lines. Given the fact that there is minor chalcopyrite and no bornite, as well as an uncertainty about the equilibrium of the Cu-minerals, we cannot precisely state an exact limit at higher values of fS_2. This is the reason why we continue the stability field with diagonal dashed lines further away.

Since there is no available thermochemical data for tetradymite (Bi_2Te_2S) we assumed that it could have formed from tellurobismuthite (Bi_2Te_3) according to the reaction: $2Bi_2Te_3 + S_2 = 2Bi_2Te_2S + Te_2$. Tetradymite could be formed at small fluctuations in fS_2 and fTe_2 as a slight S_2 fugacity increase or a subtle Te_2 fugacity decrease. It is our understanding that tetradymite stability space should be close to that of tellurobismuthite. According to previously made assumptions the stability field for the bismuthinite (Bi_2S_3) – tetradymite (Bi_2Te_2S) assemblage is approximately located along the following equilibrium line $Bi_2S_3 + 3/2Te_2 = Bi_2Te_3 + 3/2S_2$ and within pyrite chalcopyrite stability space.

Discussion and conclusions

At a minimum temperature of 230 °C, crystallization of bismuthinite, silver tellurides inclusions and argentocuprocosalite took place under minimum log fTe_2 = log fS_2 – 3.59 and maximum log fTe_2 = log fS_2 + 0.93 between log fS_2 values of –13.92 and –11.97. At higher temperatures (400 °C) the minimum Te_2 fugacity limit is given by the equation log fTe_2 = log fS_2 – 2.69 and the maximum boundary by log fTe_2 = log fS_2 + 0.68 between log fS_2 values of –8 and –3.86. Te_2 fugacity limits were constrained by the bismuthinite-hessite stability field. Although the lowest log fS_2 values are well define by cosalite appearance (–13.92 at 230 °C and –8 at 400 °C), the highest values are not. They are constrained by log fS_2 values of –11.97 at 230 °C and –3.86 at 400 °C.

The bismuthinite-tellurobismutite monovariant line has a fixed position and does not show significant changes with temperature variations. As a result, the bismuthinite-tradymite-chalcopyrite stability space is a straight forward function of the Po/Py and Cp/Bn+Py monovariant lines at high temperature and Bi_M/Bi_2S_3 and Cp/Bn+Py lines at low temperatures. Note that at 230 °C the stability field lower limit is given by the Bi_M /Bi_2S_3 line as Po/Py monovariant line would be drawn within the Bi_M space. At 230 °C and assuming that Bi-minerals crystallization took place within pyrite-chalcopyrite stability space, Bismuthinite and tellurobismutite (and probably tetradymite) log fS_2 val-

ues range between –14.63 and –11.97 while log fTe_2 values fluctuate between –13.70 and –11.04. At temperatures as high as 400 °C an increase in fS_2 (between –7.85 and –5.00) and an increase in Te_2 fugacity (between –7.17 and –4.31) is required.

The bismuth telluride inclusions trapped within bismuthinite may have formed in equilibrium with the Bi-sulfide. It is also possible that bismuthinite was the first mineral to crystallize followed by the bismuth telluride inclusions formation that may have been triggered by a slight S_2 fugacity decrease or even more likely by a Te_2 fugacity increase, possibly as a result of tellurium-rich magmatic vapor plumes.

The above data indicate that the stability fields for both mineral assemblages at a given temperature are rather similar, specially the log fS_2 values. The main difference between the NW area and SE area may not be a change in S_2 and Te_2 fugacity but a function of Pb and Cu concentration in the hydrothermal fluid. This hypothesis is consistent with the fact that galena was only found in the NW area along with cosalite but only minor chalcopyrite. On the other hand, chalcopyrite is abundant in the SE area while cosalite is rarely found and galena is absent.

It is necessary to conduct a detailed fluid inclusion study in order to constrain the temperature of formation and consequently improve the thermodynamic model. By the end of this project we hope to include all other minerals in order to make a detailed thermodynamic modeling for San Francisco de los Andes ore deposit.

References

Afifi A.M., Kelly, W.C., Essene E.J. Phase relations among tellurides, sulphides and oxides: I. Thermochemical data and calculated equilibria; II. Applications to telluride-bearing ore deposits // Economic Geology. 1988. Vol. 83. P. 377–404.

Barton, P., Skinner, B. Sulfide mineral stabilities // In: Barnes, H.L. (Eds.), Geochemistry of Hydrothermal Ore Deposits. New York, 1967. P. 236–333.

Barton, P., Skinner, B. Sulfide mineral stabilities // In: H.L. Barnes (Eds.), Geochemistry of Hydrothermal Ore Deposits. New York, John Wiley, 1979. P. 278–403.

Cardo, R., Segal S., Korzeniewski, L., Palacio, M., Chernicoff, C. Estudio metalogenetico de brechas hidrotermales portadoras de mineralizacion de Bi-Au-Cu en el ambito de la Cordillera Frontal, Provincia de San Juan // Serie de Contribuciones Tecnicas, Recursos Minerales N 31. SEGEMAR, 2008. P. 3–28 [in Spanish].

Craig, J., Barton, P. Thermochemical approximations for sulfosalts // Economic Geology, 1973. P. 493–506.

Frikken, P.H., Cooke, D.R., Walshe, J. L., Archibald, D., Skarmeta, J., Serrano, L. and Vargas, R. Mineralogical and Isotopic Zonation in the Sur-Sur Tourmaline Breccia, Rio Blanco-Los Bronces Cu-Mo Deposit, Chile: Implications for Ore Genesis // Economic Geology, 2005. Vol. 100. № 5. P. 935–961.

Garrals, R.M., Christ, C.L. Solutions, minerals, and equilibria. San Francisco. CA: Freeman, Cooper. New York, 1965. 450 p.

Krauskopf, K. B., Bird D.K. Introduction to geochemistry. 3rd edi. McGraw-Hill, New York, 1995. 647 p.

Llambias, E., Malvicini, L. The Geology and Genesis of the Bi-Cu Mineralized Breccia-Pipe, San Francisco de los Andes, San Juan, Argentina // Economic Geology, 1969. Vol. 64. P. 271–286.

Robie, R.A., Waldbaum D.R. Thermodynamic properties of minerals and related substances at 298.15 K (25.0 C) and one atmosphere (1.013 bars) pressure and at higher temperatures // US Government Printing Office, 1968. 256 p.

G.A. Tret'yakov
Institute of Mineralogy UB RAS, Miass, Russia, genatret@yandex.ru

EXTRACTION OF METALS FROM THE SEDIMENT BY THE HEATED SEAWATER: A PHYSICAL-CHEMICAL MODELING

Выполнено физико-химическое моделирование взаимодействия нагретой морской воды, осадка впадины Гуаймас и океанического габбро при соотношениях порода–морская вода (R/SW) от $1?10^{-5}$ до 10. Установлено, что максимальная экстракция железа из габбро происходит при минимальном pH и соотношении R/SW=0.007, а меди и никеля при 0.03. Кондуктивное